

Order-Disorder structural transition in a confined fluid

E. M. de la Calleja-Mora

*Instituto de Física, Universidade Federal do Rio Grande do Sul, Caixa Postal 15051,
91501-970, Porto Alegre, RS, Brazil*

Leandro B. Krott

*Campus Araranguá, Universidade Federal de Santa Catarina, Rua Pedro João Pereira, 150,
CEP 88900-000, Araranguá, SC, Brazil*

M. C. Barbosa

*Instituto de Física, Universidade Federal do Rio Grande do Sul, Caixa Postal 15051,
91501-970, Porto Alegre, RS, Brazil*

Abstract

In this paper the amorphous/solid to disorder liquid structural phase transitions of an anomalous confined fluid is analyzed using their local fractal dimension. The model is a system of particles interacting through a two length scales potentials confined by two infinite plates. In the bulk, this fluid exhibit water-like anomalies and under confinement forms layers of particles. The particle distributions of them, present different arrangements related to amorphous/solid phases. Here only the contact layer is analyzed through fractal singularity spectrum. At high densities the structural transition its quantify by the order degree to determine the phases affected by the confinement. This mapping shows that the system as the temperature increased, the fractal dimension decreases, which is consistent with the behavior studying in such systems. This result suggests that under thermodynamic perturbations, an anomalous confined liquid, presents different phase transitions achieving be characterized by its fractality.

Keywords: , Anomalous fluids, Phase transitions, Fractal dimension

1. Introduction

The characterization of the phases present in complex system is not trivial. Usually it depends in identifying the correct order parameter of the structure. For instance, the structural transformation by thermal or mechanical perturbation of fibrous, dendritic, or colloidal configurations, formed by aggregation or reaction processes have been quantified from different measures of complexity. One of these measures is the fractal dimension. The fractality is a geometrical, topological and structural property present in many natural, physics or simulated complex systems [1, 2, 3]. In many cases a fractal structure results from the kinetic aggregation of a group of particles or from the reaction processes between them [1, 4, 5] in a process that resembles a very slow nucleation and growth of mechanism. This is visually manifested by different final distributions of the particles that entails universal properties, and also influence the physical, biological or chemical properties on the system [4, 5, 6, 7, 8, 9]. These distributions can be also quantified by the mass fractal dimension that is a measure employed to quantify the different structural phase transition [10, 11, 12].

In a number of systems a single fractal dimension is unable to capture the full complexity of the system. The multi-fractal spectrum describes the scaling correlations, coexisting in the dynamical evolution of the system, at different length scales of observation. It is employed to provide a description of the aggregation kinetics. It also gives the information about how the new phase reaches the equilibrium state [3, 13, 14]. In this way the measure of the microscopic multi-scale structure through the local fractal dimension, is an important tool to identify the macroscopic state of the system, which influence the physical emergent properties.

Then, the fractal dimensions can be used as an additional tool for characterizing the complex phases emerging from phase transitions. This strategy was employed in the study of rheological fluids [15, 16], granular materials [7, 17, 18], magnetic wall domains in boracite [19] and other complex systems [11, 20, 21]. In the case of rheological systems, the final structures obtained by magnetic

particles dispersed in mineral oils and perturbed by magnetic fields show different degrees of order that were quantified by its mass fractal dimension [15]. This result was also checked experimentally [15, 17]. This structural transformations can be analyzed by glass transition approach [22, 23, 24] and is possible to identify the liquid-glass and the liquid-crystal phase transition.

All the examples cited above in which the fractal analysis were used to identify new phases were complex systems. Would this framework also be useful for describing phases in simple systems? In a simple fluid the thermodynamic and dynamic behavior is governed by the molecular length scale. This is the case of the rare gases, diatomic and triatomic molecules. In a complex fluid, the thermodynamic and dynamic properties are governed not by the atomistic length scales but by a mesoscopic scale that arises from the competition of the multi-scale molecular forces. These systems include colloidal suspensions, gels and polymer blends. Due to the complexity of the competition forces, complex fluids can be considered homogeneous at the macroscopic scale, but are disordered at the microscopic scale, and possess structure at an intermediate scale. This is the reason why the multi-fractal spectrum employed to analyze the structural transformation by mechanical perturbations can be applied in those complex fluids as well.

Water, even though a very simple triatomic molecule, is not a simple liquid. It is an anomalous material showing a number of thermodynamic and dynamic anomalies [25]. The most familiar anomaly is its increasing density with temperature, at ambient pressure, up to 4°C. Above this temperature water behaves as a normal liquid and density decreases as temperature rises. Experiments for water allow to locate the line of temperatures of maximum density (TMD) in the pressure-temperature plane. Below TMD, density decreases with decreasing temperature, differently from the behavior of the majority of fluids, for which density increases on lowering temperature [26].

In addition to the thermodynamic and dynamic anomalies, water exhibits many solid phases. Several coexistence lines separate the multiple solid phases. Thus, the energy landscape associated to the crystalline phases presents a num-

ber of sharp valleys with very low energies. The temperature and pressure ranges at which each one of these sharp valleys displays lowest energy values define the stable phase in that region of the phase diagram. Those valleys of the energy landscape that never achieve the lowest energy correspond to the amorphous configurations. When confined within plates, the fluid energy landscape becomes even more complex. The anomalous fluid forms layers and the system shows a transition from three layers to a two layers structure [27, 28, 29]. Using nanotubes, the same transition appears and it is associated with a dynamic transition from a normal to superflow regime [30, 31, 32, 33]. At low temperatures and high degree of confinement the contact layers melt, while the central layer stays liquid. The contact layer form a variety of liquid, liquid crystal and solid structures [34].

Recently a model for describing the anomalous behavior of water were studied under confinement [27]. These studies indicate that the confined system exhibits at the wall two dimensional phases not present in the bulk system [28, 34, 35, 36, 37]. While the existence of the phases is identified clearly by the instabilities of the density versus pressure phase diagram, the nature of the new structures, tested with the radial distribution function [27] and with the translational order parameter [28, 34, 35, 36, 37], it is still unclear. Particularly the system presents phases that change continuously to very different structures without phase transition while other phases change through a first order transition. These two scenarios can not be identified by the translational order parameter analysis and need further understanding.

In this work we explore the idea that the fractal analysis can provide information of the structure and phase behavior of anomalous fluids, like water. In this context we study the phase behavior of a water-like model confined within plates. The pressure versus temperature phase diagram, of this fluid is analyzed in the framework of the multi-fractal spectrum and within this framework the different phases are identified.

The paper is organized as follows: in the section II the model is introduced; in the section III the methods are presented; the results are given in the section

IV and our final conclusions are presented in the section V.

2. The Model

The water-like fluid is composed by N spherical particles of effective diameter σ that interact through a core-softened potential of two length scales, namely

$$\frac{U(r_{ij})}{\epsilon} = 4 \left[\left(\frac{\sigma}{r_{ij}} \right)^{12} - \left(\frac{\sigma}{r_{ij}} \right)^6 \right] + a \exp \left[-\frac{1}{c_0^2} \left(\frac{r_{ij} - r_0}{\sigma} \right)^2 \right] \quad (1)$$

where $r_{ij} = |\vec{r}_i - \vec{r}_j|$ is the distance between two fluid particles i and j . The first term is a standard 12-6 Lennard-Jones (LJ) potential [38] and the second one is a Gaussian well centered at r_0 , with depth a and width c_0 . The parameters used in this work are $a = 5.0$, $c_0 = 1.0$ and $r_0/\sigma = 0.7$, that result in a potential with two length scales, one around $r_{ij} \equiv r_1 \approx 1.2\sigma$ and the other at $r_{ij} \equiv r_2 \approx 2\sigma$ [39]. The potential is shown in the Figure 1(a). This model does not exhibit the directionality or explicitly hydrogen bonds as present in water, however it captures the competition between open and close water tetramers through the competition between the two length scales. As a result, the pressure versus temperature phase diagram shows a region where density, diffusion and structural properties are anomalous in bulk [40, 41, 42, 43] and in confined systems [27, 32, 33, 34, 37, 44, 45, 46, 47].

In our system the particles are confined between plates in z -direction. All simulations were done with plates of size $L_x = L_y = L = 20\sigma$, separated by a fixed distance L_z . A schematic depiction of the system is given in the Fig. 1 (b). The interaction between the fluid particles and the molecules in the plates is purely repulsive and it is given by the Weeks-Chandler-Andersen (WCA) [48] potential, namely

$$U^{\text{WCA}}(z_{ij}) = \begin{cases} 4\epsilon \left[\left(\frac{\sigma}{z_{ij}} \right)^{12} - \left(\frac{\sigma}{z_{ij}} \right)^6 \right] + \epsilon, & z_{ij} \leq 2^{1/6}\sigma, \\ 0, & z_{ij} > 2^{1/6}\sigma. \end{cases} \quad (2)$$

where z_{ij} is the distance between the plates at j position and the z -coordinate of the fluid particle i .

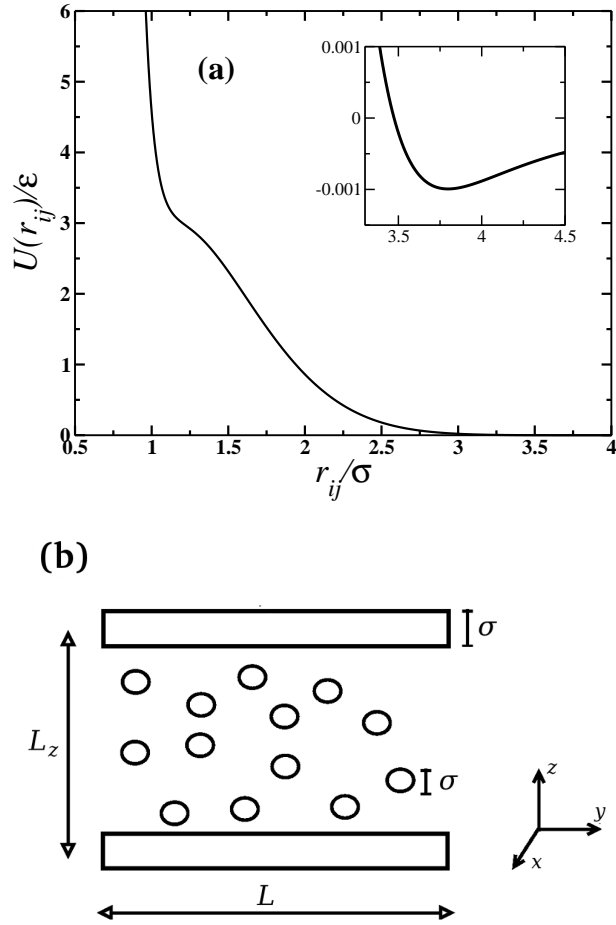


Figure 1: (a) Two length scale interaction potential and (b) schematic depiction of the confined system. The particles are confined between two flat and smooth plates, separated by a distance L_z . The energy and length scales are given by ϵ and σ , respectively.

3. Methods

3.1. The simulation details

The physical quantities are shown in reduced units [38],

$$r^* \equiv \frac{r}{\sigma} \quad \text{and} \quad \rho^* \equiv \rho \sigma^3, \quad (3)$$

for distance and density of particles, respectively, and

$$P_{\parallel}^* \equiv \frac{P_{\parallel}\sigma^3}{\epsilon} \quad \text{and} \quad T^* \equiv \frac{k_B T}{\epsilon} \quad (4)$$

for the pressure and temperature, respectively. The symbol $*$ will be omitted in order to simplify the discussion of the paper.

The molecular dynamic simulations were performed at NVT-constant. The systems have 500 particles confined between two parallel flat plates in z -direction. The plates have thickness of σ , area of L^2 and are separated by a fixed distance L_z . The value of L was 20 in all the simulations and the density of the system was changed varying the value of L_z , from 4.3 to 10.0σ .

The repulsive interaction with the plates creates an exclusion region in the z direction, consequently the total density is corrected to an effective density [49, 50]. Then the distance between the plates can be approach by $L_{ze} \approx L_z - \sigma$, resulting in an effective density of $\rho = N/(L_{ze}L^2)$. In x and y directions periodic boundary conditions were employed.

The temperature of the systems was fixed using the Nosé-Hoover heat-bath [51, 52] with a coupling parameter $Q = 2$. Simulations were performed for the temperatures ranging from $T = 0.050$ to $T = 0.450$. This choice of temperatures were made on basis of the pressure versus temperature phase diagram of the bulk system. The initial configuration was generated placing the fluid particles randomly between the plates. The equations of motion were integrated using the velocity Verlet algorithm, with time step of $\delta t = 0.001$. The systems were equilibrated with 5×10^5 steps followed by 1×10^8 steps for the production of the thermodynamic averages. A particle-particle interaction cutoff radius of $r_{\text{cut}}/\sigma = 3.5$ was used.

3.2. The multifractal spectrum

We used a standard box counting method, also called the *capacity* of the set [2, 53, 54, 55], to calculate the fractal dimension on the two-dimension configurational structure of each final equilibrium state, on the layer of the fluid confined. The images are sets of two-dimensional final stages of the simulation

process. Each one present a particle configuration for fix densities and diverse values of temperature. The procedure to measure the fractal dimension is the follow: the image is binarized by a high contrast treatment, leaving the particles black and the space between them white. A grid of four random positions cover the entire image with a decreasing size of ε as the length of the box. The scaling law to relate the number of particles and the size of the boxes follow the relation

$$N \sim \varepsilon^{-D_q} \quad (5)$$

where ε acquired successively smaller values of length until the minimum value of ε_0 and $N(\varepsilon)$ are the number of cubes required to coverall the set. The fractal dimension by the box counting method is given by

$$D_q = \lim_{\varepsilon \rightarrow 0} \frac{\ln N(\varepsilon)}{\ln(\varepsilon_0/\varepsilon)} \quad (6)$$

To describe all the statistical properties by the local fractal dimension [53, 56], we used the generalized box counting method [57, 58, 59, 60] defined as

$$D_q = \frac{1}{1-q} \lim_{\varepsilon \rightarrow 0} \frac{\ln I(q, \varepsilon)}{\ln(\varepsilon_0/\varepsilon)} \quad (7)$$

where

$$I(q, \varepsilon) = \sum_{i=1}^{N(\varepsilon)} [P_{i,q}]^q \quad (8)$$

We used the scaling exponent defined by Halsey et al. [56] as $P_{i,q}^q \sim \varepsilon_i^{\alpha q}$ where α can take a width range of values measuring different regions of the set. The spectrum generated by an infinite set of dimension $D_q = D_0, D_1, D_2, \dots$ measure the scaling structure as a function of the local pattern density. If $q=0$ the generalized fractal dimension represent the classic fractal dimension, it means that $D_f = D_{q=0}$ [61]. As the image is divided into pieces of size ε , it suggested that the number of times that α in $P_{i,q}$ takes a value between α' and $d\alpha'$ defined as $d\alpha' \rho(\alpha') \varepsilon^{-f(\alpha')}$ where $f(\alpha')$ is a continuous function. As q represents different scaling indices, we can define

$$I(q, \varepsilon) = \sum_{i=1}^{N(\varepsilon)} [P_{i,q}]^q = \int d\alpha' \rho(\alpha') \varepsilon^{-f(\alpha') + q\alpha'} \quad (9)$$

α_i is the Lipschitz-Hölder exponent, that characterizes the singularity strength in the i th box. The factor α_i allows to quantify the distribution of complexity in an spatial location. The multifractal is a set of overlapping self-similar configurations. In that way, we used the scaling relationship taking into account $f(\alpha)$ as a function to cover a length scales of observations. Defining the number of boxes as a function of the Lipschitz-Hölder exponent $N(\alpha)$, can be related to the box size ε as

$$N(\alpha) \sim \varepsilon^{-f(\alpha)} \quad (10)$$

The multi-fractal spectrum show a line of consecutive points for $Q \geq 0$ that start on the left side of the spectrum climbing up to the maximum value. Then the values for $Q \leq 0$, represented in the spectrum for a dotted line, on the right side begins to descend. The maximum value corresponds to $Q = 0$, which is equal to the box counting dimension. To obtain the multi-fractal spectrum we use the plugin *FracLac* for ImageJ[62]. Basically D_q is the variation of mass as a function of ε in the image, and give us the behavior as a power series of ε sizes distorting them by an exponent q . We select the case of $D_f = D_{q=0}$ as the parameter of order in the images. In the plugin we select four grid positions that cover the total image, and the mode scaled series was selected to see the singularity spectrum results. The final configuration of the simulations, present a particle distribution of particles in black. The parameters of the program were calibrate for this kind of images.

4. Results

The temperature versus density phase diagram of this system was obtained by molecular dynamic simulations [27] showing the various two dimensional phases present at the contact layer.

The existence of phase transitions in the analysis of Bordin et al. [27] was obtained by computing the density versus pressure isochores and observing instabilities related to first-order phase transitions. The general classification employed for by Bordin et al [27] for defining the different phases of this system

took into account: the radial distribution function, the particles mobility and a snapshot of the system. It is interesting to observe that large structural changes can occur without phase transition. In order to understand how very different structures are connected here we explore the fractal dimension of each one of these structures.

Now let us explore each density region of the phase diagram. Figure 2 (a) illustrates the temperature versus total density phase diagram showing the different phases present at the fluid contact layer [27]. Figure 2 (b) show selected snapshots of the different phases. At this high density region at low temperatures a liquid-crystal phase (I) coexists with a solid hexagonal phase (II). At higher values of the temperature both phases become liquid and increasingly disordered and for $\rho_{c3} = 0.321$ and $T_{c3} = 0.45$ the coexistence disappears at critical point. It is important to notice that no phase transition is observed between the liquid-crystal phase: phase I, and the liquid phases: phases III and V. Also no phase transition is observed between the solid hexagonal phase, phase II, and the other two liquid phases, phases IV and VI.

Here we complement this analysis by identifying the different phases with the correlation between each final equilibrium state of the phase transition and the degree of ordering.

The starting point for our analysis are the snapshots of the system. Fig. 2 (b) shows the pictures for the temperatures $T = 0.075$ (points I and II), $T = 0.200$ (points III and IV) and $T = 0.350$ (points V and VI). These figures represent the final equilibrium state in which the specific structure exists. To make more evident this evolution, we calculated the fractal dimension of each layer at those different densities and temperatures. This order parameter gives a quantitative classification for these phase transitions.

Figure 3(a) presents the maximum values obtained in the singularity spectrum as a function of total density, ρ , while figure 3(b) shows it as a function of the separation between plates, L_z , for the three values of the temperature. In all the cases the fractal dimension increases with the increasing of confinement. Since the fractal dimension can be used as measure of the degree of order [1, 15],

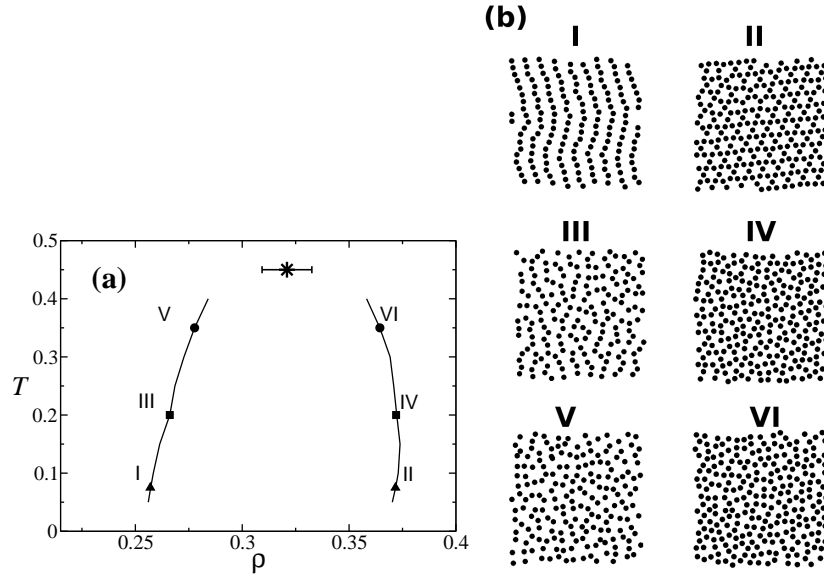


Figure 2: (a) Temperature versus total density phase diagram for high densities. The star represents the critical point at $T_c = 0.450$ and $\rho_c = 0.321$. The solid lines delimitate the coexistence region between liquid-crystal and hexagonal solid phases. The triangles, squares and circles are isochores at $T = 0.075, 0.200$ and 0.350 , respectively, and densities $\rho_{I,III,V} \approx 0.260$, $\rho_{II,IV,VI} \approx 0.370$. The corresponding snapshots of the contact layer are shown in (b). More details in the text.

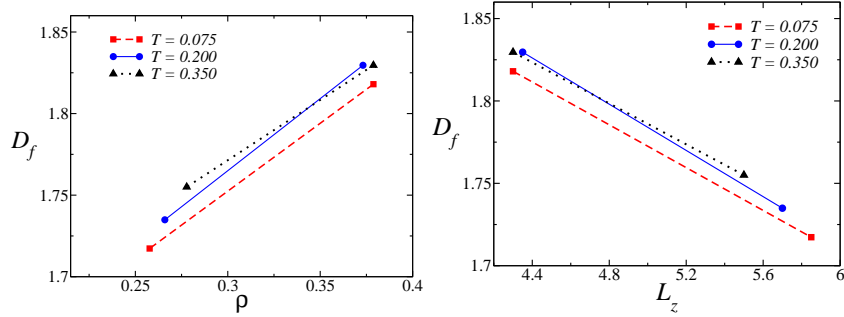


Figure 3: (a) Fractal dimension as function of (a) total density and (b) separation of plates for transition at high densities.

our results confirm that for each temperatures the order increases with density. It is interesting to notice that, the slopes of the constant temperature lines are

almost the same for all the temperatures analyzed, indicating that even though the structures change with temperature, the difference in order between the low density and high density structures, change proportionally. In addition, the values of the fractal dimension of the phases I, III and V are very similar, while the values for phases II, IV and VI are almost the same. This could explain why the transformation between them requires no phase transition.

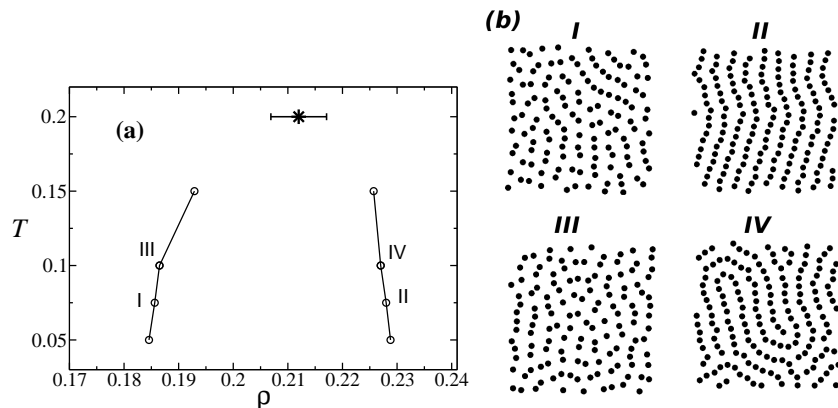


Figure 4: (a) Temperature versus total density phase diagram for intermediate densities. The star represents the critical point at $T_c = 0.20$ and $\rho_c = 0.212$. The solid lines delimitate the coexistence region between dimeric liquid and liquid-crystal phases. The snapshots of the contact layer are shown in (b) for the points I and II at $T = 0.075$ and for points III and IV at $T = 0.100$, with densities $\rho_{I,III} \approx 0.185$ and $\rho_{II,IV} \approx 0.228$.

Fig. 4(a) illustrates the temperature versus density phase diagram of the liquid at the contact layer of the confined system in a region of intermediate densities [27]. At low temperatures a liquid-crystal phase (II) coexists with a structured liquid phase (I) made of dimers. When the temperature is raised both the liquid-crystal and the structured dimeric liquid becomes disordered, phases (IV) and (III) in the Fig. 4(b) respectively. As the temperature is increased even further the coexistence ends at a critical point at $T_{c2} = 0.20$ and $\rho_{c2} = 0.212$. It is important to notice that even though quite different in structure it is possible to go from the phase I to phase III and from phase II to phase IV with no phase

transition.

The snapshots of the final states of the system at the contact layer for this intermediate range of densities are depicted in the Figure 4(b). The figure illustrates the states I and II at $T = 0.075$ and for III and IV $T = 0.100$, with densities $\rho_{I,III} \approx 0.185$ and $\rho_{II,IV} \approx 0.228$, respectively. Employing these

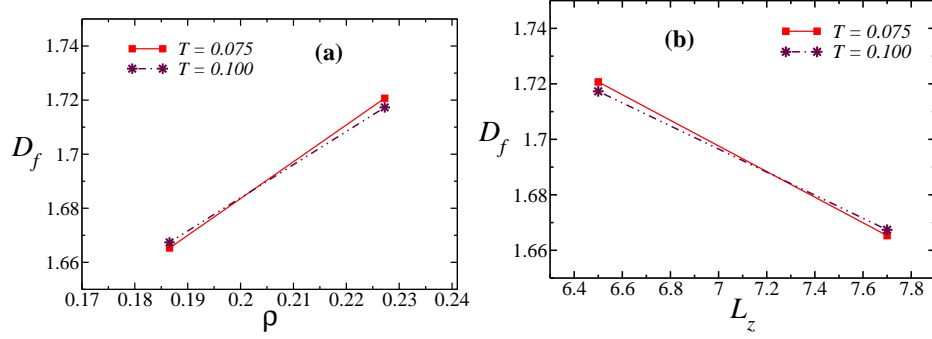


Figure 5: (a) Fractal dimension as function of (a) total density and (b) separation of plates for transition at intermediate densities.

snapshots, the fractal dimensions of these configurations were computed. The Figure 5 shows the degree of ordering evolution as a function of total density and of the distance L_z for this intermediate region of densities. Similarly to what happens at high densities shown in Fig. 3 the increase in the confinement and the decrease of the distance between the wall leads to an increase in the order. The phases I and III show almost the same value for the fractal dimension. The same occurs for the phases II and IV. This result support the idea that the transformation from one phase to another structurally very different with no phase transition might be related to our findings that they share the same fractal structure.

Figure 6(a) shows the temperature versus density phase diagram of the liquid at the contact layer of the confined system in a region of low densities [27] showing liquid configurations at coexistence. The coexistence between the two liquid phases ends at a critical point at $T_{c1} = 0.125$ and $\rho_{c1} = 0.158$. The snap-

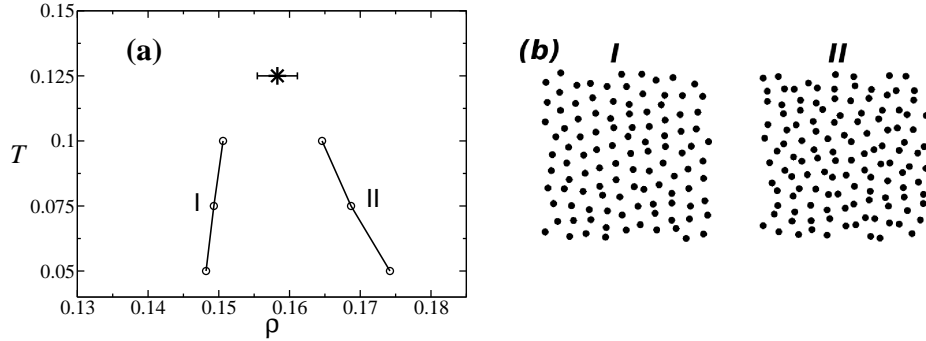


Figure 6: (a) Temperature versus total density phase diagram for low densities. The star represents the critical point at $T_c = 0.125$ and $\rho_c = 0.158$. The solid lines delimitate the coexistence region between disordered liquid and dimeric liquid phases. The snapshots of the contact layer are shown in (b) for the points I and II at $T = 0.075$, with densities $\rho_I \approx 0.149$ and $\rho_{II} \approx 0.169$.

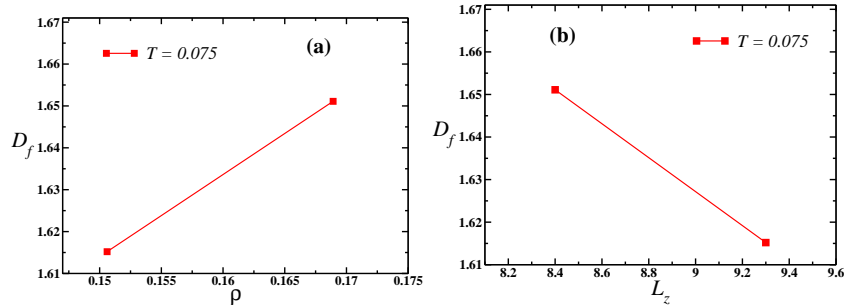


Figure 7: Fractal dimension as function of (a) density for $T = 0.075$ and (b) separation between plates.

shots of representative phases at the contact layer are shown in the Figure 6(b). Phases *I* and *II*, with $T = 0.075$ and densities $\rho_I \approx 0.149$ and $\rho_{II} \approx 0.169$ are illustrated, respectively.

These equilibrium configurations were employed to compute the fractal dimension of the system. In the Fig. 7(a), we show the fractal dimension as function of density, while in the Figure 7 (b) the fractal dimension is computed as a function of the separation between plates. At this temperature, the disorder degree varies from $D_f = 1.6152$ ($\rho \approx 0.150$) to $D_f = 1.6511$ ($\rho \approx 0.170$). Even

all the configurations being liquid states, we identify different degree of disorder in each case.

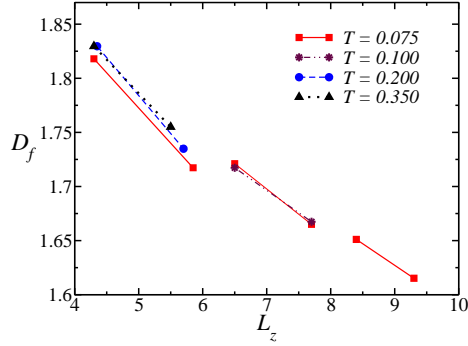


Figure 8: Order evolution as function of L_z for all the cases studied.

In all the densities analyzed the fractal analysis confirms the results obtained with molecular dynamic simulations. Now in order to check if the different phase transitions show drastic differences in the evolution of the fractal dimension, the degree of ordering is compared. Figure 8 illustrates the fractal dimension as a function of the distance between the plates, L_z for all the cases studied here. The fractal dimension not only increases with the density but also a drastic change of slope is observed at very high densities. This region of pressures and temperatures represents the solid to liquid phase transitions where a high degree of ordering is expected confirming the suggestions of the molecular dynamic simulations.

5. Conclusion

In this work we have explored the use of the fractal dimension to analyze the phases present in an anomalous fluid confined by repulsive walls.

The degree of configurational order-disorder of the confined liquid was analyzed using the fractal spectrum approach through image analysis. We found that different phases separated by phase transitions show a very different fractal dimension that increases with the increasing order of the structure of the phase. Complementary to this result we also found that phases that are not

separated by phase transitions show a very similar fractal dimension. This result sheds some light on the odd possibility of a continuous transition between two structurally very different phases.

6. Acknowledgment

We thank the Brazilian agencies CNPq, INCT-FCx, and Capes for the financial support. E.M.D.C. Bolsista do CNPq - Brazil.

References

- [1] T. Vicsek, *Fractal Growth Phenomena* (World Scientific, Singapore, 1989).
- [2] M. F. Barnsley, *Fractals Everywhere*, (Academic Press Professional, United States of America, 1993).
- [3] B. Mandelbrot, *The Fractal Geometry of Nature* (W.H. Freeman and Company, New York, 1977).
- [4] J. L. Carrillo, F. Donado, and M. E. Mendoza, Phys. Rev. E **68**, 061509 (2003).
- [5] P. Meakin, Adv. in Coll. and Inter. Sci. **28** 249-331 (1988).
- [6] P. Meakin, Phys. Rev. Lett. **51**, 11191122 (1983).
- [7] D. L. Blair and A. Kudrolli, Phys. Rev. E **67**, 021302 (2003).
- [8] M. Matsushita and H. Fujikawa, Phys. A, **168** 498 (1990).
- [9] E. Ben-Jacob, O. Shochet, A. Tenenbaum, I. Cohen, A. Czirok, and T. Vicsek, Nature, **368** 46 (1994).
- [10] R. C. Ball, D. A. Weitz, T. A. Witten, and F. Leyvraz, Phys. Rev. Lett. **58** 3 (1987).
- [11] T. A. Witten and L. M. Sander, Phys. Rev. Lett. **47** 14001403 (1981).

- [12] A. Snezhko, I. S. Aranson, and W.-K. Kwok, Phys. Rev. Lett. **94** 108002 (2005).
- [13] E. Bacry, F. Muzy, and A. Arnodo, J. Stat. Phys. **70** (1993)
- [14] A. Chhabra, and R. V. Jensen, Phys. Rev. Lett. **62**, 1327 (1989).
- [15] E. M. de la Calleja Mora, J. L. Carrillo, M. E. Mendoza and F. Donado, Eur. Phys. J. B. **86**, 1126 (2013).
- [16] E.M. de la Calleja, J. L. Carrillo, F. Donado, Rev. Mex. de Fs. **58** 54-57 (2012).
- [17] J. Gonzalez-Gutierrez, J. L. Carrillo-Estrada and J. C. Ruiz-Suarez, J. Stat. Mech. **12** 12015 (2013).
- [18] P. Pusey, *Freezing and Glass Transition* (J.P. Hansen, D. Levesque, J. Zinn-Justin (Eds.), Elsevier Science, Amsterdam, 1991).
- [19] R. E. Moctezuma, J. L. Carrillo, and M. E. Mendoza, Rev. Mex. de Fs. S **58** 4853 (2012).
- [20] M. Suzuki, Progr. of Theor. Phys. **69** 1 (1983).
- [21] J. González-Gutiérrez, J.L. Carrillo-Estrada, O. Carvente, and J.C. Ruiz-Suárez, Eur. Phys. J. E **37** 37 (2014).
- [22] P.G. Debenedetti and F.H. Stillinger, Nature, **410**, 259 (2001).
- [23] M.S. Shell and P.G. Debenedetti, Phys. Rev. E **69** 051102 (2004).
- [24] F.H. Stillinger and P.G. Debenedetti, Annu. Rev. Cond. Matter Phys., **4** 263 (2013).
- [25] M. Chaplin, Seventy two anomalous properties of water, www1.lsbu.ac.uk/water/water_anomalies.html, 2015.
- [26] C. A. Angell, E. D. Finch, L. A. Woolf, and P. Bach, J. Chem. Phys. **65**, 3063 (1976).

- [27] J. R. Bordin, L. B. Krott, and M. C. Barbosa, *J. Phys. Chem. C* **118**, 9497 (2014).
- [28] L. B. Krott, J. R. Bordin, N. B. Marçal Jr. and M. C. Barbosa, *J. Chem. Phys.* **142** 134502(2015).
- [29] N. Giovambattista, P. J. Rossky, and P. G. Debenedetti, *Phys. Rev. Lett.* **102**, 050603 (2009).
- [30] S. Jakobtorweihen, M. G. Verbeek, C. P. Lowe, F. J. Keil, and B. Smit, *Phys. Rev. Lett.* **95**, 044501 (2005).
- [31] X. Qin, Q. Yuan, Y. Zhao, S. Xie, and Z. Liu, *Nanoletters* **11**, 2173 (2011).
- [32] J. R. Bordin, A. Diehl, and M. C. Barbosa, *J. Phys. Chem. B* **117**, 7047 (2013).
- [33] J. R. Bordin, J. S. Soares, A. Diehl, and M. C. Barbosa, *J. Chem Phys.* **140**, 194504 (2014).
- [34] J. R. Bordin, L. B. Krott and M. C. Barbosa, *J. Chem. Phys.* **141**, 144502 (2014).
- [35] J. R. Errington and P. G. Debenedetti, *Nature (London)* **409**, 318 (2001).
- [36] Y. D. Fomin, V. N. Ryzhov, B. A. Klumov and E. N. Tsiok, *J. Chem Phys.* **141**, 034508 (2014).
- [37] L. B. Krott, J. R. Bordin, and M. C. Barbosa, *J. Phys. Chem. B* **119**, 291 (2015).
- [38] P. Allen and D. J. Tildesley, *Computer Simulation of Liquids*, (Oxford University Press, Oxford, 1987).
- [39] A. B. de Oliveira, E. Salcedo, C. Chakravarty, and M. C. Barbosa, *J. Chem. Phys.* **132**, 234509 (2010).
- [40] A. B. de Oliveira, P. A. Netz, T. Colla, and M. C. Barbosa, *J. Chem. Phys.* **124**, 084505 (2006).

- [41] A. B. de Oliveira, P. A. Netz, T. Colla, and M. C. Barbosa, *J. Chem. Phys.* **125**, 124503 (2006).
- [42] G. S. Kell, *J. Chem. Eng. Data* **12**, 66 (1967).
- [43] C. A. Angell, E. D. Finch, and P. Bach, *J. Chem. Phys.* **65**, 3063 (1976).
- [44] J. R. Bordin, A. B. de Oliveira, A. Diehl, and M. C. Barbosa, *J. Chem. Phys.* **137**, 084504 (2012).
- [45] L. B. Krott and M. C. Barbosa, *J. Chem. Phys.* **138**, 084505 (2013).
- [46] L. B. Krott and J. R. Bordin, *J. Chem. Phys.* **139**, 154502 (2013).
- [47] L. B. Krott and M. C. Barbosa, *Phys. Rev. E* **89**, 012110 (2014).
- [48] J. D. Weeks, D. Chandler, and H. C. Andersen, *J. Chem. Phys.* **54**, 5237 (1971).
- [49] P. Kumar, S. V. Buldyrev, F. Sciortino, E. Zaccarelli, and H. E. Stanley, *Phys. Rev. E* **72**, 021501 (2005).
- [50] P. Kumar, F. W. Starr, S. V. Buldyrev, and H. E. Stanley, *Phys. Rev. E* **72**, 011202 (2007).
- [51] W. G. Hoover, *Phys. Rev. A* **31**, 1695 (1985).
- [52] W. G. Hoover, *Phys. Rev. A* **34**, 2499 (1986).
- [53] E. Ott, *Chaos in Dynamical Systems*, (Cambridge University Press, United States of America, 1993).
- [54] A. Chhabra, R. V. Jensen, *Phys. Rev. Lett.* **62** 1327 (1989).
- [55] A. B. Chhabra, C. Meneveau, R. V. Jensen, and K. R. Sreenivasan, *Phys. Rev. A* **40**, 5284 (1989).
- [56] T. C. Halsey, M. H. Jensen, L. P. Kadanoff, I. Procaccia, N. I. Shraiman, *Phys. Rev. A* **33** 1141 (1986).

- [57] G. E. Hentschel, I. Procaccia, *Physica* **8D** 435 (1983).
- [58] M.J. Feigenbaum, M.H. Jensen, I. Procaccia, *Phys. Rev. Lett.* **57**, 1503 (1986).
- [59] P. Grassberger, *Phys. Lett. A* **97**, 227 (1983)
- [60] H.G.E. Hentschel and I. Procaccia, *Physica D* **8**, 435 (1983)
- [61] J. R. Mureika, G. C. Cupchik and C. C. Dyer, *Leonardo* **37** 53-56 (2004).
- [62] T. Ferreira and W. Rasband, *ImageJ user guide*, <http://rsb.info.nih.gov/ij/docs/guide/user-guide.pdf>, 2013.